JACS
JOURNAL OF THE AMERICAN CHEMICAL SOCIETY

ARTICLE

pubs.acs.org/JACS

Steric Control of the Donor/Acceptor Interface: Implications in Organic Photovoltaic Charge Generation

Thomas W. Holcombe,[†] Joseph E. Norton,[#] Jonathan Rivnay,[⊥] Claire H. Woo,[‡,§] Ludwig Goris,[⊥,▽] Claudia Piliego,[§] Gianmarco Griffini,[§,○] Alan Sellinger,[⊥] Jean-Luc Brédas,[#] Alberto Salleo,[⊥] and Jean M. J. Fréchet*[,†,‡,§,∥]

[†]Department of Chemistry, and [‡]Department of Chemical Engineering, University of California Berkeley, Berkeley, California 94720-1460, United States

[§]Materials Sciences Division, Lawrence Berkeley National Laboratory, Berkeley, California 94720, United States

[∥]King Abdullah University of Science and Technology, Thuwal, Saudi Arabia 23955-6900

[⊥]Department of Materials Science and Engineering, Stanford University, Stanford, California 94305, United States

[#]Center for Organic Photonics and Electronics and School of Chemistry and Biochemistry, Georgia Institute of Technology, Atlanta, Georgia 30332, United States

[▽]Institute for Materials Research (IMO), Hasselt University, Diepenbeek, Belgium

[○]Department of Chemisty, Politecnico di Milano, 20133 Milan, Italy

Supporting Information

ABSTRACT: The performance of organic photovoltaic (OPV) devices is currently limited by modest short-circuit current densities. Approaches toward improving this output parameter may provide new avenues to advance OPV technologies and the basic science of charge transfer in organic semiconductors. This work highlights how steric control of the charge separation interface can be effectively tuned in OPV devices. By introducing an octylphenyl substituent onto the investigated polymer backbones, the thermally relaxed charge-transfer state, and potentially excited charge-transfer states, can be raised in energy. This decreases the barrier to charge separation and results in increased photocurrent generation. This finding is of particular significance for nonfullerene OPVs, which have many potential advantages such as tunable energy levels and spectral breadth, but are prone to poor exciton separation efficiencies. Computational, spectroscopic, and synthetic methods were combined to develop a structure−property relationship that correlates polymer substituents with charge-transfer state energies and, ultimately, device efficiencies.

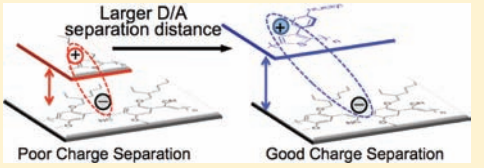

INTRODUCTION

State-of-the-art solution processable organic photovoltaic (OPV) devices generally rely on fullerene derivatives as both the electron acceptor and the electron transporter.[1] Fullerene: polymer blends, termed bulk heterojunctions (BHJs), hold record efficiencies around 8%.[2] Although these devices have provided exceptional growth for the field of OPVs and have demonstrated rapid performance improvement over the past two decades, alternative n-type materials[3] and device architectures[4] could lead to "break-through" technological and basic science advances. Currently, the best nonfullerene OPV device efficiencies hover around 2%.[5] To move beyond fullerene-based OPVs, a greater understanding of charge generation in organic photovoltaics is critical.

Fullerenes provide several potential advantages over polymers and nonfullerene small molecules in photovoltaic applications: they possess high molecular symmetry,[6] are strongly polarizable, and present triply degenerate LUMO levels.[7] Conjugated polymers and planar small molecules are less symmetric, often have well-defined charge-transport axes,[8] and are generally not as highly polarizable overall; conjugated polymers have a dielectric constant of ca. 3[9a] versus fullerenes with a dielectric constant of ca. 4.[9b] These properties of fullerenes generally facilitate charge separation and the generation of free carriers.

Because OPVs require a donor/acceptor interface to separate the photoexcited state (Frenkel-type excitons),[10] it is important to understand the thermodynamics of charge separation at this interface.[1d,11] The relative free energy of charge separation (ΔG_{CS}^{rel}) for several donor materials combined with a fullerene acceptor has previously been estimated by the abbreviated Weller equation $\Delta G_{CS}^{rel} = E_s - |(HOMO_{donor} - LUMO_{acceptor})|$, where the difference between the singlet excited state energy (E_s) and the relative band offsets provided good agreement with measured short-circuit current (J_{sc}).[12] Although values for ΔG_{CS}^{rel} calculated from this equation correlated with the observed J_{sc} for several devices,[12,13] other factors such as active layer absorption breadth, optical density, morphology, as well as charge-carrier mobility and electrode choice are all known to critically affect J_{sc} in addition to ΔG_{cs}. A brief description of how

Received: April 8, 2011
Published: June 20, 2011

morphology can specifically impact charge separation is presented in the Supporting Information, and it is discussed with reference to the current investigation. Notably, the abbreviated Weller equation does not include the lattice polarization energy or Coulomb attraction terms, as these are not easily measured.[14] Toward expanding our understanding of charge generation in OPVs, we must explore factors beyond the thermodynamics of charge separation as estimated from bulk electronic properties.

For instance, charge generation depends not only on the donor and acceptor material state energies, but also on the specific molecular environment at the donor/acceptor (D/A) interface and on the kinetics of exciton separation/recombination.[15,11] Akin to a chemical reaction, exciton separation to yield free charges can proceed via more than one mechanism. In some cases, no "reaction intermediates" are observed, whereas in other cases there is a spectroscopically observable "geminate pair" or charge transfer (CT) state. Probing the parameters that control the mechanism of charge generation, particularly for nonfullerene devices, is of great importance to the field of OPVs. Studies show that this electron−hole (e−h) pair is sensitive to applied electric field and, intriguingly, to hydrostatic pressure: an externally applied field during device operation is known to increase the current extracted from the device; when the bias is applied opposite ("reverse") to the voltage generated under illumination, free carriers are quickly removed from the active layer, and the dipolar geminate pair is driven to separate.[16] External pressure on the system is believed to have the opposite effect on the geminate pair, decreasing the intermolecular distance at the D/A interface, and leading to increased radiative recombination of the CT state with a lower energy, implying a more stable, deeply trapped intermediate.[17]

Our work toward understanding charge generation started from a structural point of view, and we drew inspiration from studies reported by Granstrom et al. in 1998.[18] In that publication, poly[3-(4-*n*-octyl)-phenylthiophene] (POPT) was shown to produce the most photocurrent in any OPV device at the time, a notable achievement with the common electron acceptor material poly[2-methoxy-5-(2′-ethylhexyloxy)-1,4-(1-cyanovinylene)phenylene] (CNPPV). Motivated by that research, we reported studies in which (POPT) outperformed poly(3-hexylthiophene) (P3HT) in both bilayer devices with CNPPV[5b] and BHJ devices with the newer acceptor material 4,7-bis(2-(1-(2-ethylhexyl)-4,5-dicyanoimidazol-2-yl)vinyl)benzo[*c*][1,2,5]-thiadiazole (EV-BT).[5c] Our first report focused on the inconsistency between expected and realized performance values for OPV devices with the acceptor CNPPV, specifically the almost double short-circuit current density (J_{sc}) for POPT devices despite reduced optical density as compared to P3HT; however, very little was understood at that time about why better performance was achieved with POPT instead of P3HT. In our second report, we utilized EV-BT to make progress toward elucidating the physical properties that governed the OPV performance parameters of these nonfullerene devices. For example, reverse bias analysis suggested a tighter binding of the geminate pair at the P3HT:EV-BT interface; that is, a lower-energy CT state provided a deeper energetic well (a trapped intermediate) for partially separated charges. We suspected that the octylphenyl content of POPT played a critical role at the D/A interface, potentially facilitating geminate pair separation.

To shed light on how using an alkylphenyl side group enhances J_{sc} as compared to a simple alkyl side group, we investigated analogous material combinations with different substitution and acceptor materials. Beyond correlating structure to performance on the basis of multiple device comparisons, more direct methods to investigate

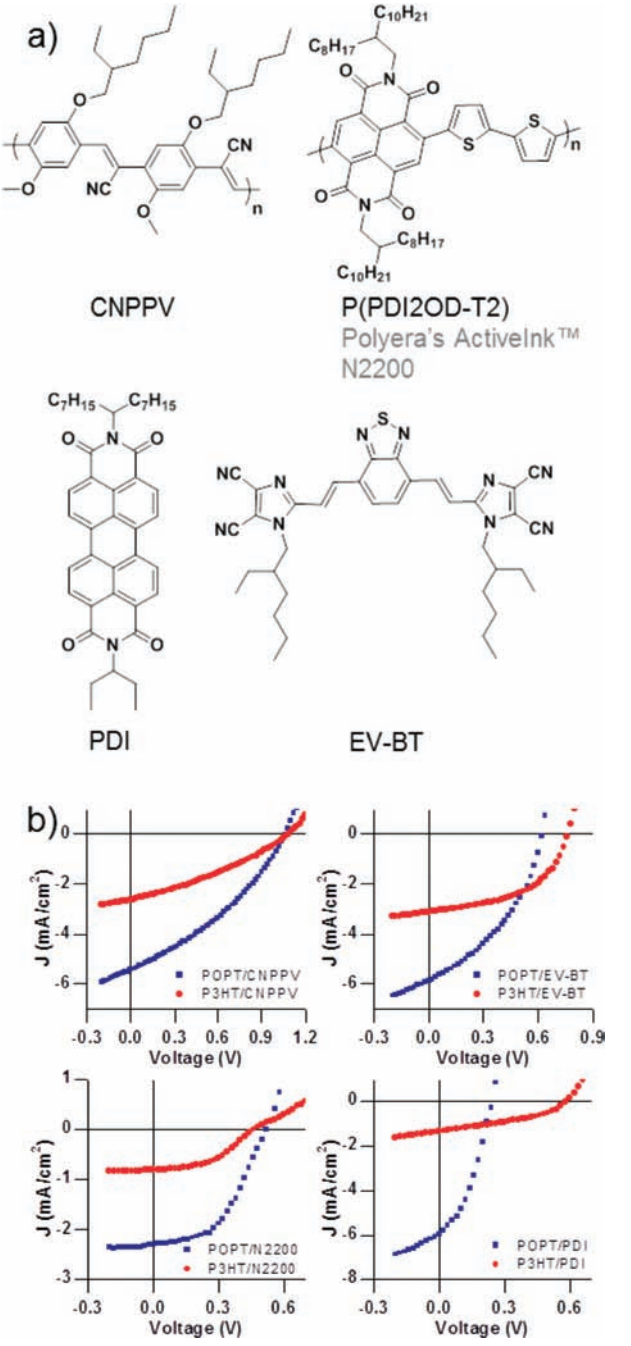

Figure 1. (a) Structures of P3HT and POPT, (b) the structures of four different acceptors (two polymers and two small molecules) that are tested in a head-to-head comparison between P3HT and POPT. (c) $J-V$ curves for the devices corresponding to the acceptor components in (a).

the CT states were necessary to draw a fitting conclusion. Herein, we utilize a combination of computational and spectroscopic methods, as well as tailored synthesis and extensive device engineering, to understand how modifying thiophene substitution from alkyl to octylphenyl on two otherwise identical backbones, polythiophene and polyquarterthiophene, leads to a greater understanding of the effects that side group interactions at D/A interfaces have on charge generation. Structural control of the D/A interface may prove to be a powerful tool for tuning charge separation dynamics, and we

Table 1. PV Output Characteristics of POPT versus P3HT Devices, and Maximum Efficiencies for Optimized Device Systems[a]

device active layer	J_{sc} [mA/cm^2]	V_{oc} [V]	FF	PCE [%]
POPT/CNPPV	−5.44	1.06	0.35	2.00
P3HT/CNPPV	−2.63	1.08	0.33	0.93
POPT:EV-BT	−5.70	0.62	0.40	1.41
P3HT:EV-BT	−2.81	0.77	0.51	1.11
POPT/N2200	−2.50	0.52	0.47	0.61
P3HT/N2200	−0.80	0.46	0.46	0.17
POPT:PDI	−5.70	0.24	0.37	0.51
P3HT:PDI	−1.70	0.57	0.41	0.39

[a] Symbol "/" indicates a bilayer device, while symbol ":" indicates a BHJ device. Devices were optimized first on the basis of thickness (solvent choice and solution concentration) and then on the basis of annealing conditions (various temperatures and times).

provide a seminal example of how steric effects can improve charge separation in organic photovoltaics.

RESULTS

Both P3HT and POPT were synthesized via the GRIM polymerization method.[5b] The structure of POPT consists of phenyl groups covalently bound to the polythiophene backbone as part of the solubilizing substituent. This functionality increases the ionization potential (deepens the HOMO level) to −5.5 eV from −5.2 eV as compared to P3HT. Additionally, the optical properties are shifted toward a broader spectral response while maintaining similar charge-transport properties.[5b] The energetic changes result in an excited state that is lower in energy (and the electron affinity is also more exothermic) in POPT as compared to P3HT; thus, POPT is thermodynamically less likely to undergo exciton separation with a given acceptor, as compared to P3HT (when a normal Marcus regime can be invoked). Contrary to thermodynamic expectations, however, POPT yielded more efficient charge separation as a donor material in PV cells with polymeric and small molecule acceptors, such as CNPPV and EV-BT, respectively.[5b,c] In particular, the considerably and recurrently higher J_{sc} prompted an in-depth investigation combining device fabrication, theoretical modeling, and advanced spectroscopy to gain insight into these systems. The following results exploit observed differences in performance caused by the presence of phenyl substituents to better understand the charge separation process. By expanding our data set beyond the two systems already reported,[5b,5c] we aim to probe the universality of this design strategy for improving charge generation in nonfullerene OPVs.

Four acceptors were utilized with POPT and P3HT in head-to-head comparisons: CNPPV, EV-BT, *N*-(1-hexylheptyl)-*N*′-(1-ethylpropyl)perylene-3,4,9,10-tetracarboxylic diimide (PDI),[19] and poly{[*N*,*N*′-bis(2-octyldodecyl)-naphthalene-1,4,5,8-bis(dicarboximide)-2,6-diyl]-*alt*-5,5′-(2,2′-bithiophene) (Polyera ActiveInk N2200),[20] Figure 1a (see the Supporting Information for device fabrication details). In most cases, both bilayer and bulk heterojunction devices were compared, provided that an orthogonal solvent system was found to allow the fabrication of bilayers; here, we report the device architecture that demonstrated the higher efficiencies for each acceptor material. Polymer−polymer solar cells performed better in the bilayer device architecture, whereas polymer−small molecule solar cells were better in the BHJ architecture. On the basis of individually optimized devices in all four comparisons, POPT consistently outperforms P3HT (Table 1 and Figure 1b). While the V_{oc} and FF of the POPT and P3HT devices are comparable in most cases, the J_{sc} values of POPT devices are at least twice those of P3HT devices, leading to the higher overall efficiencies of POPT devices. It should be noted that the P3HT/N2200 device results are consistent with two recent reports that demonstrated N2200 in a BHJ device with P3HT yields ∼0.2% efficiency.[21] Additionally, the kink observed for the P3HT/N2200 device may be due to similar effects discussed in prior work.[16b] The effect of morphology on J_{sc}, generally and in the cases of POPT/CNPPV and P3HT/CNPPV devices, is discussed in the Supporting Information.

To generalize the effect of interfacial steric interactions on charge generation, we expanded the scope of this study beyond POPT and P3HT to another polymer backbone, polyquarterthiophene. We synthesized poly(3,3-di(4-*n*-octyl)phenylquaterthiophene) PQT-OP and compared it to poly(3,3-didodecylquaterthiophene) PQT-DD (Table 2 and Figure 2). Independently optimized devices with CNPPV, EV-BT, and PDI were consistently found to perform nearly twice as well with PQT-OP than PQT-DD, due largely to an increase in J_{sc}. The V_{oc} values for PQT-based devices with the same

Table 2. PV Output Characteristics of PQT-OP versus PQT-DD Devices[a]

device active layer	J_{sc} [mA/cm^2]	V_{oc} [V]	FF	PCE [%]
PQT-OP/CNPPV	−2.43	1.18	0.39	1.12
PQT-DD/CNPPV	−1.51	1.20	0.38	0.69
PQT-OP/EV-BT	−2.68	0.95	0.48	1.22
PQT-DD/EV-BT	−1.48	0.98	0.43	0.62
PQT-OP:PDI	−3.33	0.63	0.42	0.88
PQT-DD:PDI	−2.18	0.66	0.34	0.49

[a] Reported are maximum efficiencies for individually optimized device systems. A "/" indicates a bilayer device, while a ":" indicates a BHJ device.

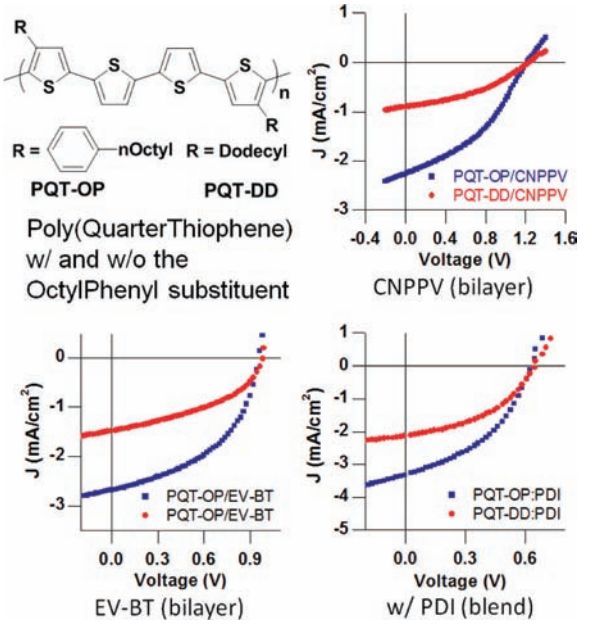

Figure 2. PQT polymer structures and a comparison of individually optimized devices. Devices were optimized first on the basis of thickness (solvent choice and solution concentration) and then on annealing conditions (various temperatures and times).

acceptor material were greater than for the polythiophene-based; however, there were no significant V_{oc} differences between the phenyl and alkyl PQT derivatives. This lends credence to the hypothesis that interfacial interactions could play a role that rivals the importance of the materials state energies.[22,23] The CT state energy, whatever its physical structure, has already been strongly correlated with V_{oc}.[22] It is worth noting that PQT-OP provides PDI-based devices with the highest performance to date. These data supported our hypothesis that the effect of this substituent could be generalized to other systems, as this is the same trend that was observed for POPT as compared to P3HT.

These experimental results are in contradiction with predictions based on a simple comparison of the donor polymer state energies. The larger ionization potential (lower HOMO level) of POPT as compared to P3HT (−5.5 vs −5.2 eV) in combination with a smaller bandgap should thermodynamically result in a lower J_{sc} based on the abbreviated Weller equation. However, octylphenyl devices produce significantly increased J_{sc} values as compared to devices utilizing the alkyl analogues. Morphological and light absorption parameters were ruled out in previous studies as the dominant factor in this kind of comparison, through a careful examination of device output parameters during optimization and analysis (such as reverse-bias analysis), as well as characterization of the films by AFM.[5b,c] Examination of the PQT polymers provided similar results. PQT-OP has a slightly larger ionization potential (IP) and a similar optical gap as compared to PQT-DD; PQT-OP and PQT-DD have IPs of −5.4 versus −5.3 eV, respectively, and optical gaps of approximately 1.9−2.0 eV (with absorption onsets of 640 and 620 nm). Again, devices using the octylphenyl-containing donor polymers consistently produce a substantially greater J_{sc}. These data clearly confirm that the material state energies and optical properties are not the only factors affecting the charge generation efficiencies in these systems. More importantly, we hypothesize that the molecular interactions at the D/A interface are a determining factor in these devices. Modeling of the D/A interface has recently predicted that the molecular configurations[23] and environment at this interface are critical in the charge-generation process, and here we aim to correlate theory with a benchmark physical test system.[15,24]

Because the highest performing devices utilized POPT and P3HT in combination with CNPPV (Table 1, Figure 1) as the component materials, these systems were characterized in more detail to understand how their structural properties influence interfacial interactions and, ultimately, charge generation. The component materials were first analyzed using a computational description of their molecular geometries. Modeling at the Density Functional Theory (DFT) B3LYP/6-31G(d,p) level of theory provided optimized geometries of the neutral ground states for (isolated) hexamers of the relevant species (Figure 3). Two POPT conformations were explored: the first structure allows the phenyl rings to participate in conjugation with the thiophene backbone (Figure 3b, POPT-*unconstrained*), and the second structure forces the phenyl rings to twist perpendicular to the backbone (Figure 3c, POPT-*perp*). POPT-*perp* minimizes conjugation between the pendant phenyl ring of the side group and the thiophene ring of the polymer backbone but maximizes conjugation along the backbone (see Supporting Information, Figure S1). The neutral ground-state geometries were also calculated for P3HT (Figure 3a) and CNPPV (Figure 3d), where the alkyl chains were modeled as methyl groups. The calculations show that the backbone of POPT is strictly planar only when the phenyl rings are forced out of plane with respect to the backbone, minimizing steric or electronic interactions between the thiophene and phenyl groups.

Vertical transition energies of the polymers can be qualitatively described from those of the oligomers by a Kuhn-type dependence on $1/N$ where N is the number of double bonds along the shortest path connecting the terminal carbon atoms of the molecular backbone.[25] The electronic structures for oligomers of increasing length were calculated, and a Kuhn fit of the data was used to extrapolate the $S_0 \rightarrow S_1$ transition energies of the extended polymers. The plots for the two POPT structures, P3HT, and CNPPV are presented in Figure 4. The best agreement between theory and experiment, that is, where the optical bandgap (E_g^{opt}) for POPT equals 1.8 eV, occurs when the polymer backbone is planar, suggesting that the phenyl groups of polymer side chains prefer to orient perpendicular to the backbone in thin films. The results for P3HT and CNPPV are also in good agreement with experiment.

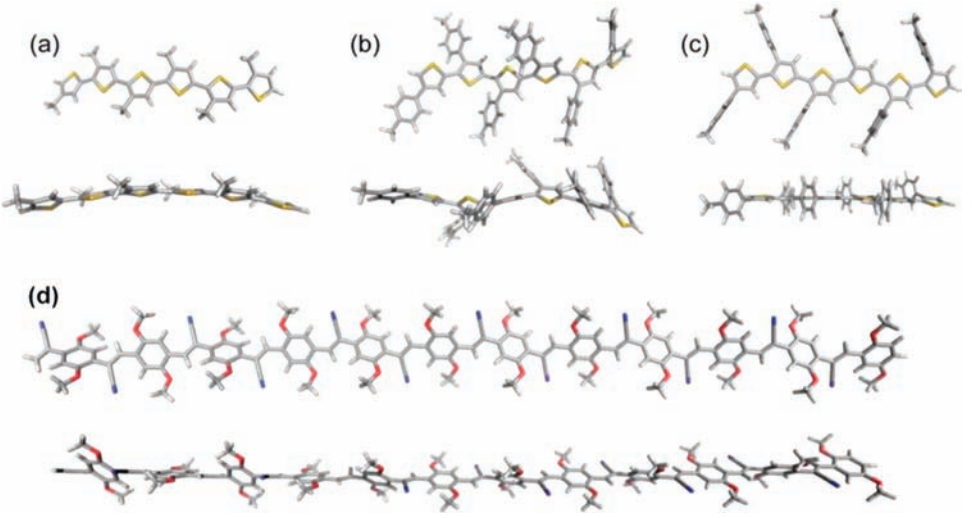

Figure 3. B3LYP/6-31G(d,p)-optimized neutral ground-state structures of the hexamers of (a) P3HT, (b) POPT-*unconstrained*, (c) POPT-*perp*, and (d) CNPPV shown from the top-view (top) and side-view (bottom).

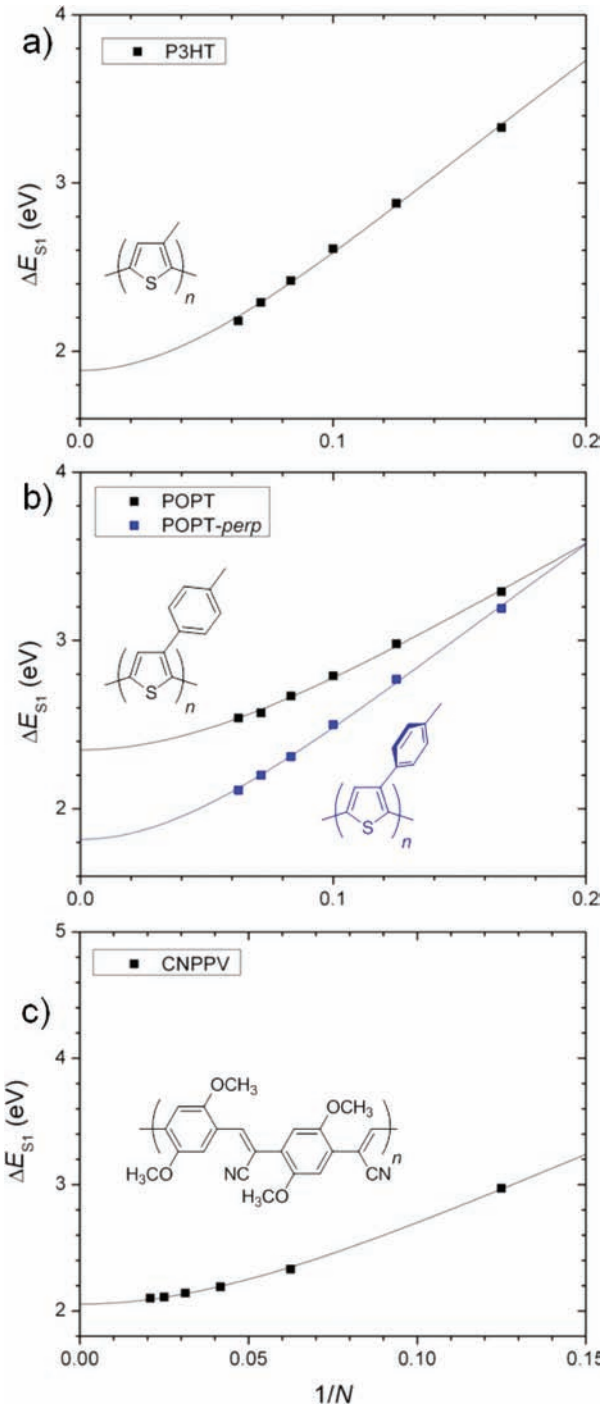

Figure 4. Vertical S0 → S1 transition energies of (a) P3HT and (b) POPT-*unconstrained* and POPT-*perp* where the phenyl group is constrained to be perpendicular to the polymer backbone (c) CNPPV. *N* is the number of double bonds along the backbone.

The presence of two dominant conformations of POPT is supported empirically by two-dimensional grazing incidence X-ray scattering (2D GIXS) measurements. Figure 5a shows the 2D GIXS pattern and the in-plane line scan of the POPT sample, while Figure 5b illustrates the schematic of solid-state packing for POPT. The presence of two peaks at 3.8 and 5.1 Å suggests that there are two different $\pi-\pi$ packing distances in the POPT thin film. Importantly, these two different $\pi-\pi$ packing distances arise from the two major conformations for the phenyl rings relative to the POPT backbone: the $\pi-\pi$ packing distance of 3.8 Å correlates to the phenyl ring oriented parallel with the backbone, while the $\pi-\pi$ stacking distance of 5.1 Å correlates to a POPT-*perp* orientation where the phenyl ring is twisted perpendicular to the backbone and causes an increase in separation between adjacent polymers. It should also be noted that the peak broadening observed in the GIXS pattern may be an indication that the phenyl ring can adopt varying degrees of rotation between the parallel and perpendicular conformations. The packing parameters of POPT and several phenyl-substituted polythiophenes have been studied in-depth elsewhere.[26] GIXS data of PQT-OP also evidence two dominant conformations for the phenyl ring, resulting in $\pi-\pi$ spacings of 5.1 and 3.9 Å (Supporting Information, Figure S2). The relative scattering intensity of the two $\pi-\pi$ spacings in PQT-OP is reversed from that of POPT. This reversal in PQT-OP can be attributed to the lack of substituents on two of the four thiophenes in the polymer repeat unit, thereby favoring the tighter $\pi-\pi$ spacing at 3.9 Å. Detailed GIXS data for P3HT[27] and PQT-DD[28] have been analyzed previously, and backbone spacings of 3.8 and 4.2 Å were reported, respectively. CNPPV derivatives are known to be relatively amorphous; however, weak diffraction signals between 4 and 5 Å have been observed.[29] X-ray scattering is limited to the investigation of regular periodicity present in a bulk material, and it is not appropriate for the study of polymer blend or bilayer interfaces. However, as the D/A interface in these material systems was our primary focus, we turned to computational analysis to develop a model interface for the charge separation event.

Model dimer configurations were constructed from best-fit planes of polythiophene/CNPPV separated at distances (*R*) between 4 and 5 Å in 0.2 Å increments (Figure 5d). To construct CT states from these dimers, charges were constrained to each molecule using the constrained density functional theory (C-DFT) method implemented in NWChem Version 4.6.[30] A conductor polarizable continuum model (CPCM) with $\varepsilon = 4$ was used to approximate polarization effects expected in organic solid-state systems. Given the limitations of the theoretical approach, we are mainly interested in the relative CT-state energies, which are plotted in Figure 5c. The model dimer configuration of POPT-*perp* is predicted to have the highest CT state energy followed by the P3HT and then the POPT-*unconstrained* configurations. PQT-OP model calculations require many more nuclei at the interface, which is beyond the scope of the present work.

To verify our calculations of the CT state energies in these D/A systems, we used spectroscopic techniques to experimentally observe their CT states. Sensitive photocurrent measurements, via Fourier transform photocurrent spectroscopy (FTPS),[22,24b] can extract the weak sub-bandgap external quantum efficiency, and photothermal deflection spectroscopy (PDS) can detect sub-bandgap absorption. These tools have previously been used to investigate charge-transfer states.[31] A recent and very significant FTPS study suggests that the CT state, sometimes called a CT exciton, is very efficiently split into free charge carriers at room temperature in P3HT:PCBM and MDMO-PPV:PCBM devices.[32] Spectral evidence and device studies of various D/A systems suggest that these CT states determine the V_{oc} of the PV cell and act as an intermediate in the generation and recombination of free charge carriers.[22,24b] Consequently, spectroscopic techniques rooted in sub-bandgap absorption are considered a good indicator

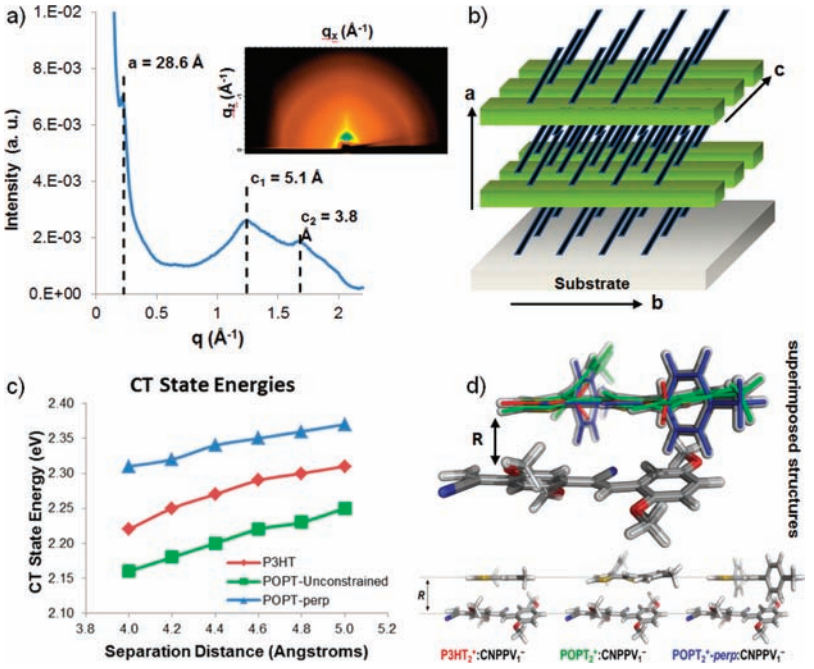

Figure 5. (a) An X-ray line scan taken parallel to the substrate surface showing peaks at *d* spacing equal to 28.6, 5.1, and 3.8 Å corresponding to the "*a*" distance and two different "*c*" distances, respectively, taken from the 2D GIXS pattern of POPT on Si substrate (inset). (b) Schematic of the polymer packing relative to the substrate, with corresponding labels to the peaks indicated in (a). (c) CT-state energies for the D/A systems illustrated in (d), estimated at the C-DFT B3LYP/6-31G(d,p) level. (d) Physical representation of dimers of POPT and P3HT with a single repeat unit of CNPPV, both superimposed and side-by-side.

of the presence of such CT states and of the maximum V_{oc} that can be expected with a given D/A combination.

Here, PDS spectra were obtained by detecting the mirage effect in a transparent, inert medium (Fluorinert) with a probe HeNe laser beam. Nonradiative heating associated with absorption of a monochromatic pump beam causes the mirage effect to occur. PDS was used in this investigation to support our hypothesis that molecular orientation of the phenyl groups affects the CT state energy. PDS measurements were performed on drop cast and spun cast films of POPT and P3HT blended with CNPPV. We underline here that bilayer films do not provide enough interfacial surface area to produce good signal-to-noise ratios; in addition, the molecular level interface is not expected to change upon going from the bilayer to BHJ morphology, vide infra, and see extended discussion in the Supporting Information. Figure 6 shows the PDS spectra of the homopolymers and the polymer blends under investigation; spectra are scaled to absolute values of the absorption coefficient by matching the signal near the absorption edge to that from the UV−vis spectra of the same films.

Blends of both P3HT and POPT with CNPPV produce nonadditive absorptions that are attributed to the presence of CT states at the D/A interfaces. For P3HT:CNPPV (1:1 wt/wt), a CT state absorption is present at 1.26 eV. For POPT, however, there are two sub-bandgap peaks attributed to CT states, one at 1.17 eV and one at 1.50 eV, possibly indicating two distinct interfacial configurations. These peak maxima are extracted by fitting an exponential for the band edge and Gaussian curves for the CT peaks in the sub-bandgap regions. The results of the calculations presented in Figure 5c are qualitatively in agreement with the observed PDS absorption peaks, in that the P3HT:CNPPV blend has a CT state energy that resides between the two POPT:CNPPV CT state energies. (We note that, in addition to the intrinsic limitations of the methodologies, the difference in energy between theory and experiment may be due in part to the fact that the physical size of the CT state (e.g., the extent that the CT exciton is delocalized) could be larger than what was considered in the calculations.) To verify that the energies of these CT states remain unchanged with film morphology and film thickness, POPT:CNPPV (1:1) films were compared as both drop cast and spun cast from 1,2-dichlorobenzene (Supporting Information, Figure S3). While the CT state peak positions do not change, the relative intensity of the sub-bandgap absorption to the UV−vis absorption is enhanced in the spun cast film, likely a result of finer scale phase segregation that leads to greater D/A interfacial surface area and increased relative sub-bandgap absorption.

PDS measurements were also performed to probe the CT state energies of the PQT-based polymers blended with CNPPV. The PQT-DD:CNPPV (1:1 wt/wt) shows little nonadditive sub-bandgap absorption, while PQT-OP presents two sub-bandgap absorption peaks at 1.25 and 1.56 eV. The higher energy CT state peak is significantly less intense for PQT-OP as compared to POPT (Supporting Information, Figure S4); the reason for this is discussed below. It should be noted that our first attempts to obtain a clean PDS signal from PQT polymers were difficult until we discovered that residual palladium from the cross-coupling polymerization led to an erroneous mirage effect and dramatically increased background signal (Figure S5).

DISCUSSION

A thermodynamic driving force for charge generation, that is, exciton dissociation leading to charge separation, is present at the interface between the donor/acceptor (D/A) materials in an

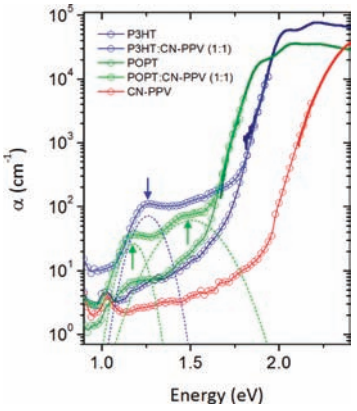

Figure 6. Absorption spectra of P3HT, POPT, and blends with CN-PPV. Thick solid lines are UV−vis absorption spectra of the homopolymers; symbols are the PDS absorption spectra of drop cast films. The arrows indicate the sub-bandgap features attributed to CT states in the blend systems. P3HT:CNPPV peak maximum at 1.26 eV, while POPT:CNPPV possesses two peaks at 1.17 and 1.50 eV.

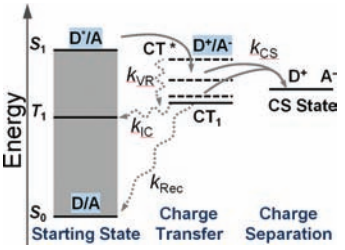

Figure 7. A diagram of possible electron flow pathways at the D/A interface, relative to potential energy (adapted from ref 11). CT state energies (ground-state solid black, excited-state dashed black) are shown in relation to the D/A singlet excited state (S_1), triplet state (T_1), and ground state (S_0). Competing energetic pathways and rates are also depicted: vibrational relaxation of the CT state (k_{VR}), intersystem crossing of the CT state to the donor triplet state (k_{IC}), recombination of the CT state to the ground state (k_{Rec}), and finally charge separation (k_{CS}). In addition to thermodynamics considerations, the kinetics of these processes will determine the charge separation behavior for each photovoltaic system.

OPV active layer. Photon absorption by either the donor or the acceptor materials produces the opportunity for charge-carrier generation: in the case of "donor" excitation, the system decreases in potential energy from the singlet excited state (E_s) by transferring an electron from donor to acceptor, and in the case of "acceptor" excitation, by transferring a hole from acceptor to donor. For simplicity, the process is generally discussed from the viewpoint of an excited donor material. A general diagram depicting charge separation is presented in Figure 7.

Although a thermodynamic driving force helps to generate free charges, the immediate physical separation of the electron and hole does not necessarily lead directly to free charges. The low dielectric constant of the active layer can produce a Coulomb trap for a partially separated exciton at the D/A interface. This state is usually referred to as a charge-transfer (CT) state. The CT state may either recombine to the initial ground states of the donor and acceptor materials or undergo further separation into free charges. It is broadly debated whether an intermediate CT state is requisite to charge separation,[11,32] and it is more recently debated whether this separation/generation can occur from lowest-lying CT_1 states.[32] It was also recently reported that a modest thermodynamic driving force of 0.1 eV leads to reasonable quantum yields of photocurrent with fullerene-based devices, based on commonly measured material properties, which supports our previous finding with POPT/CNPPV.[34] The contention surrounding the lowest-lying CT states is that they can be bound (vs the charge-separated states) by more energy than thermally available from k_BT (where k_B is the Boltzmann constant); thus, it is postulated that excess energy released during partial exciton dissociation could create higher-lying (excited) CT states (CT*), which are more likely to escape the Coulomb trap.[33c] However, strictly discussing the thermodynamics of charge separation ignores the important kinetic considerations of this process.

The efficiency of the charge separation (CS) process indeed depends on kinetic factors. Given that there is greater potential energy stored in the singlet exciton than a charge transfer exciton, and the possibility that sub-bandgap absorption produces excited CT* states that may relax down to CT_1, two rates are of critical importance: the rate of charge separation (k_{CS}) and the rate of vibrational relaxation of an excited CT state down to CT_1 (k_{VR}); see Figure 7. If $k_{CS} > k_{VR}$, then the electron is expected to readily escape the Coulomb potential and proceed to the CS state. If $k_{VR} > k_{CS}$, then relaxation to the CT_1 state leads to a more tightly bound (lower energy) intermediate. The electron can still escape from this state;[32] however, other processes start to compete with charge separation: if either the donor or the acceptor material possesses a triplet level (T_1) below the CT_1 state, intersystem crossing leads to long-lived metastable triplets. Also, the CT_1 state for some systems can radiatively or vibrationally decay to the ground state S_0.[16c,35] For these reasons, the kinetics of CS must be considered when parsing the charge-generation process.

In this work, OPV devices comparing POPT to P3HT and PQT-OP to PQT-DD were fabricated and analyzed. POPT and PQT-OP possess phenyl groups covalently bound to the polymer backbone as part of the solubilizing substituents. This functionality decreases the thermodynamic driving force for charge separation (vide supra), but both POPT and PQT-OP produced remarkably higher J_{sc} relative to their alkyl analogs. All relevant PV characteristics are summarized in Tables 1 and 2. Further, X-ray scattering data evidenced that both POPT and PQT-OP may adopt planar-with- and perpendicular-to-the-backbone conformations for the pendant phenyl rings. CT state energies for model dimer configurations were calculated and are plotted in Figure 5c: POPT-*perp* is predicted to have the highest CT state energy, while the CT state energy for P3HT lies between those of the POPT-*perp* and POPT-*unconstrained* conformations. Finally, experimental spectroscopic evidence of charge-transfer states at the interface with the acceptor CNPPV, gathered via PDS for all four donor polymers, is consistent with the relative values predicted by the model dimer calculations.

With an out-of-plane twist of the phenyl rings, the separation distance between POPT and the acceptor molecule would likely increase as steric repulsion from the phenyl rings hinders backbone−backbone interaction. PDS data confirm the presence of two distinct features in the sub-bandgap regime, which could be a direct result of these two dominant conformations at the D/A interface, as it has been explained in the previous section. Because these conformationally dependent states are both involved as intermediates in the charge-generation process, the corresponding geminate pairs would overcome different energetic barriers to split into free charges. We postulate that a twisted phenyl ring

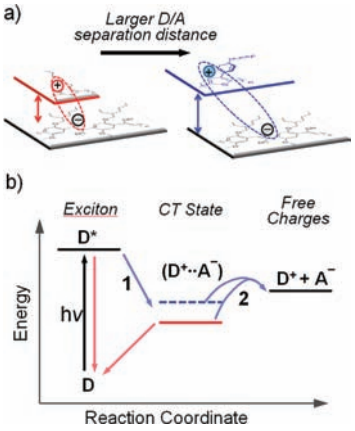

Figure 8. (a) Cartoon of how steric interactions can lead to an increase in backbone spacing, a decrease in the Coulomb binding force, and destabilization of the geminate pair. (b) Schematic of how the change depicted in cartoon (a) leads to a different energy landscape with increased charge separation probability in POPT, as the CT state is considered an intermediate trapped in an energetic well.

conformation of POPT (POPT-*perp*) is beneficial for charge generation, as an intermediate with increased potential energy is more likely to fully separate into free charges (Figure 8). FTPS measurements could lead to a quantitative description of the quantum yields for these two states, and this is the focus of future work.

This study also generated two additional significant and supportive findings. PDI-based acceptors have garnered much attention as alternative n-type materials to replace fullerenes;[3a] here, we produce the highest efficiency devices with this acceptor to date, despite tremendous efforts with alternative approaches toward higher efficiency.[3a,13a,19] This is just another indication that control over the interfacial geometry at the molecular level can lead to much improved device performance, as a complementary tool to morphology and state energy control. Additionally, the photovoltaic performance with the high mobility n-type polymer ActiveInk N2200 demonstrates that POPT outperforms P3HT both in our laboratories and as compared to two very recent reports.[21]

Combining all of the data, analysis, and literature context, we have synthesized and proposed a general design principle for improved charge separation in nonfullerene OPVs: tuning the D/A interfacial interaction through steric control to facilitate photocurrent generation. Regardless of whether charge separation happens from a relaxed CT_1 state or an excited CT state, increasing the steric bulk at the D/A interface likely decreases the Coulomb binding strength exerted on the geminate pair. We postulate that the phenyl ring pendant to POPT and PQT-OP provides an almost ideal interaction distance between the charge carrying components of the D/A interface, and this leads to two of the best nonfullerene devices to date. The higher energy of the intermediate CT state, with a lower activation barrier to free carrier generation, improves photocurrent generation and provides the key to the observed phenomenon (Figure 8). This effect was not limited to one donor polymer or one acceptor material, but rather it was general for two donors and four acceptors (four polymers and two small molecules), for a total of seven material combinations. All of these material combinations yielded optimized devices with the phenyl containing polymeric substituents producing substantially greater photocurrents, and overall power conversion efficiencies, than the alkyl analogues.

CONCLUSIONS

We have utilized computational modeling, PDS spectroscopy and tailored synthetic design to probe the importance of steric interactions at the donor/acceptor interface in nonfullerene OPV devices. By introducing the octylphenyl substituent onto the investigated polymer backbones, the thermally relaxed charge-transfer state, and potentially excited charge-transfer states, are likely raised in energy, as evidenced by PDS. This decreases the barrier to charge separation, and assuming we have controlled properly for changes in morphology by thoroughly optimizing each materials/device system, it could be the source of increased photocurrent generation. The design principle was shown to be general across two polythiophene backbones and with four different acceptors, two polymers and two small molecules. Additionally, the lower energy PDS onset for POPT-based devices with CNPPV (1.17 eV) versus the onset for PQT-OP with CNPPV (1.26 eV) is reflected in the V_{oc} of these devices. The combined data from POPT and PQT-OP devices and their materials analyses suggest that controlling the steric interaction at the D/A interface could be a general design principle toward improving charge generation in nonfullerene OPVs.

ASSOCIATED CONTENT

Supporting Information. Experimental, device fabrication, and characterization details. This material is available free of charge via the Internet at http://pubs.acs.org.

AUTHOR INFORMATION

Corresponding Author
frechet@berkeley.edu

ACKNOWLEDGMENT

This work was supported by the Center for Advanced Molecular Photovoltaics (Award No. KUS-C1-015-21), supported by King Abdullah University of Science and Technology (KAUST), and the U.S. Department of Energy under Contract No. DE-AC02-05CH11231 (synthesis and some device characterization work). T.W.H., C.H.W., and J.R. thank the National Science Foundation for graduate research fellowships. We gratefully acknowledge Polyera Inc. and Paul Armstrong for providing the Active Ink N2200 and PDI, respectively, used in this study. Paul Armstrong and Yoshi Miyamoto are thanked for assistance with device optimization. We also thank David Kavulak and Barry Thompson for helpful discussions.

REFERENCES

(1) (a) Boudreault, P. T.; Najari, A.; Leclerc, M. *Chem. Mater.* **2011**, *23*, 456–459. (b) He, Y. J.; Chen, H. Y.; Hou, J. H.; Li, Y. F. *J. Am. Chem. Soc.* **2010**, *132*, 1377–1382. (c) Piliego, C.; Holcombe, T. W.; Douglas, J. D.; Woo, C. H.; Beaujuge, P. M.; Frechet, J. M. J. *J. Am. Chem. Soc.* **2010**, *132*, 7595–7597. (d) Thompson, B. C.; Frechet, J. M. J. *Angew. Chem., Int. Ed.* **2008**, *47*, 58–77.

(2) Chen, H. Y.; Hou, J. H.; Zhang, S. Q.; Liang, Y. Y.; Yang, G. W.; Yang, Y.; Yu, L. P.; Wu, Y.; Li, G. *Nat. Photonics* **2009**, *3*, 649–653.

(3) (a) Anthony, J. E. *Chem. Mater.* **2010**, *23*, 583–590. (b) Brunetti, F. G.; Gong, X.; Tong, M.; Heeger, A. J.; Wudl, F. *Angew. Chem., Int. Ed.* **2010**, *49*, 532–536. (c) Shin, R. Y. C.; Kietzke, T.; Sudhakar, S.; Dodabalapur, A.; Chen, Z. K.; Sellinger, A. *Chem. Mater.* **2007**, *19*, 1892–1894.

(4) Lee, M. R.; Eckert, R. D.; Forberich, K.; Dennler, G.; Brabec, C. J.; Gaudiana, R. A. *Science* **2009**, *324*, 232–235.

(5) (a) McNeill, C. R.; Abrusci, A.; Zaumseil, J.; Wilson, R.; McKiernan, M. J.; Burroughes, J. H.; Halls, J. J. M.; Greenham, N. C.; Friend, R. H. *Appl. Phys. Lett.* **2007**, *90*, 1935061–3. (b) Holcombe, T. W.; Woo, C. H.; Kavulak, D. F. J.; Thompson, B. C.; Frechet, J. M. J. *J. Am. Chem. Soc.* **2009**, *131*, 14160–14161. (c) Woo, C. H.; Holcombe, T. W.; Unruh, D. A.; Sellinger, A.; Frechet, J. M. J. *Chem. Mater.* **2010**, *22*, 1673–1679. (d) Zhou, E.; Cong, J.; Wei, Q.; Tajima, K.; Yang, C.; Hashimoto, K. *Angew. Chem., Int. Ed.* **2011**, *50*, 2799–2803.

(6) The fullerene structure is a truncated icosohedron.

(7) Kanai, Y.; Grossman, J. C. *Nano Lett.* **2007**, *7*, 1967–1972 and references therein.

(8) Wöll, C. *Physical and Chemical Aspects of Organic Electronics: From Fundamentals to Functioning Devices*; Wiley-VCH: Weinheim, 2008.

(9) (a) Knipper, M.; Parisi, J.; Coakley, K.; Waldauf, C.; Brabec, C. J.; Dyakonov, V. *Z. Naturforsch., A* **2007**, *62*, 490–494. (b) Mihailetchi, V. D.; Koster, L. J. A.; Blom, P. W. M.; Melzer, C.; de Boer, B.; van Duren, J. K. J.; Janssen, R. A. J. *Adv. Funct. Mater.* **2005**, *15*, 795–801.

(10) (a) Sariciftci, N. S.; Smilowitz, L.; Heeger, A. J.; Wudl, F. *Science* **1992**, *258*, 1474–1476. (b) Halls, J. J. M.; Walsh, C. A.; Greenham, N. C.; Marseglia, E. A.; Friend, R. H.; Moratti, S. C.; Holmes, A. B. *Nature* **1995**, *376*, 498–500.

(11) Bredas, J. L.; Norton, J. E.; Cornil, J.; Coropceanu, V. *Acc. Chem. Res.* **2009**, *42*, 1691–1699.

(12) Ohkita, H.; Cook, S.; Astuti, Y.; Duffy, W.; Tierney, S.; Zhang, W.; Heeney, M.; McCulloch, I.; Nelson, J.; Bradley, D. D. C.; Durrant, J. R. *J. Am. Chem. Soc.* **2008**, *130*, 3030–3042.

(13) (a) Shoaee, S.; Clarke, T. M.; Huang, C.; Barlow, S.; Marder, S. R.; Heeney, M.; McCulloch, I.; Durrant, J. R. *J. Am. Chem. Soc.* **2010**, *132*, 12919–12926. (b) Clarke, T. M.; Ballantyne, A. M.; Nelson, J.; Bradley, D. D. C.; Durrant, J. R. *Adv. Funct. Mater.* **2008**, *18*, 4029–4035.

(14) Morteani, A. C.; Sreearunothai, P.; Herz, L. M.; Friend, R. H.; Silva, C. *Phys. Rev. Lett.* **2004**, *92*, 2474021–4.

(15) Beljonne, D.; Cornil, J.; Muccioli, L.; Zannoni, C.; Bredas, J. L.; Castet, F. *Chem. Mater.* **2011**, *23*, 591–609.

(16) (a) Marsh, R. A.; Hodgkiss, J. M.; Friend, R. H. *Adv. Mater.* **2010**, *22*, 3672–3676. (b) Ooi, Z. E.; Tam, T. L.; Sellinger, A.; deMello, J. C. *Energy Environ. Sci.* **2008**, *1*, 300–309. (c) Veldman, D.; Ipek, O.; Meskers, S. C. J.; Sweelssen, J.; Koetse, M. M.; Veenstra, S. C.; Kroon, J. M.; van Bavel, S. S.; Loos, J.; Janssen, R. A. J. *J. Am. Chem. Soc.* **2008**, *130*, 7721–7735.

(17) Schmidtke, J. P.; Friend, R. H.; Silva, C. *Phys. Rev. Lett.* **2008**, *100*, 1574011–4.

(18) Granstrom, M.; Petritsch, K.; Arias, A. C.; Lux, A.; Andersson, M. R.; Friend, R. H. *Nature* **1998**, *395*, 257–260.

(19) Rajaram, S.; Armstrong, P. B.; Kim, B. J.; Frechet, J. M. J. *Chem. Mater.* **2009**, *21*, 1775–1777.

(20) Yan, H.; Chen, Z. H.; Zheng, Y.; Newman, C.; Quinn, J. R.; Dotz, F.; Kastler, M.; Facchetti, A. *Nature* **2009**, *457*, 679–686.

(21) (a) Fabiano, S.; Chen, Z.; Vahedi, S.; Facchetti, A.; Pignataro, B.; Loi, M. A. *J. Mater. Chem.* **2011**, ASAP. (b) Moore, J. R.; Albert-Seifried, S.; Rao, A.; Massip, S.; Watts, B.; Morgan, D. J.; Friend, R. H.; McNeill, C. R.; Sirringhaus, H. *Adv. Energy Mater.* **2011**, *1*, 230–240.

(22) Vandewal, K.; Tvingstedt, K.; Gadisa, A.; Inganas, O.; Manca, J. V. *Nat. Mater.* **2009**, *8*, 904–909.

(23) (a) Yi, Y. P.; Coropceanu, V.; Bredas, J. L. *J. Am. Chem. Soc.* **2009**, *131*, 15777–15783. (b) Yi, Y.; Coropceanu, V.; Bredas, J. L. *J. Mater. Chem.* **2011**, *21*, 1479–1486.

(24) (a) Huang, Y. S.; Westenhoff, S.; Avilov, I.; Sreearunothai, P.; Hodgkiss, J. M.; Deleener, C.; Friend, R. H.; Beljonne, D. *Nat. Mater.* **2008**, *7*, 483–489. (b) Vandewal, K.; Tvingstedt, K.; Gadisa, A.; Inganas, O.; Manca, J. V. *Phys. Rev. B* **2010**, *81*, 1252041–8.

(25) Gierschner, J.; Cornil, J.; Egelhaaf, H. J. *Adv. Mater.* **2007**, *19*, 173–191.

(26) Fell, H. J.; Samuelsen, E. J.; Mardalen, J.; Andersson, M. R. *Synth. Met.* **1995**, *69*, 283–284.

(27) Verploegen, E.; Mondal, R.; Bettinger, C. J.; Sok, S.; Toney, M. F.; Bao, Z. A. *Adv. Funct. Mater.* **2010**, *20*, 3519–3529.

(28) Thompson, B. C.; Kim, B. J.; Kavulak, D. F.; Sivula, K.; Mauldin, C.; Frechet, J. M. J. *Macromolecules* **2007**, *40*, 7425–7428.

(29) (a) Chen, S. A.; Chang, E. C. *Macromolecules* **1998**, *31*, 4899–4907. (b) Chen, S. H.; Su, C. H.; Su, A. C.; Chen, S. A. *J. Phys. Chem. B* **2004**, *108*, 8855–8861.

(30) (a) Wu, Q.; Van Voorhis, T. *J. Chem. Theory Comput.* **2006**, *2*, 765–774. (b) Wu, Q.; Van Voorhis, T. *J. Phys. Chem. A* **2006**, *110*, 9212–9218. (c) Wu, Q.; Van Voorhis, T. *Phys. Rev. A* **2005**, *72*, 0245021–4. (d) Valiev, M.; Bylaska, E. J.; Govind, N.; Kowalski, K.; Straatsma, T. P.; Van Dam, H. J. J.; Wang, D.; Nieplocha, J.; Apra, E.; Windus, T. L.; de Jong, W. *Comput. Phys. Commun.* **2010**, *181*, 1477–1489.

(31) (a) Goris, L.; Haenen, K.; Nesladek, M.; Wagner, P.; Vanderzande, D.; De Schepper, L.; D'Haen, J.; Lutsen, L.; Manca, J. V. *J. Mater. Sci.* **2005**, *40*, 1413–1418. (b) Goris, L.; Poruba, A.; Hod'akova, L.; Vanecek, M.; Haenen, K.; Nesladek, M.; Wagner, P.; Vanderzande, D.; De Schepper, L.; Manca, J. V. *Appl. Phys. Lett.* **2006**, *88*, 0521131–3.

(32) Lee, J.; Vandewal, K.; Yost, S. R.; Bahlke, M. E.; Goris, L.; Baldo, M. A.; Manca, J. V.; Van Voorhis, T. *J. Am. Chem. Soc.* **2010**, *132*, 11878–11880.

(33) (a) Clarke, T. M.; Durrant, J. R. *Chem. Rev.* **2010**, *110*, 6736–6767. (b) Deibel, C.; Strobel, T.; Dyakonov, V. *Adv. Mater.* **2010**, *22*, 4097–4111. (c) Zhu, X. Y.; Yang, Q.; Muntwiler, M. *Acc. Chem. Res.* **2009**, *42*, 1779–1787.

(34) Zhou, Y.; Tvingstedt, K.; Zhang, F. L.; Du, C. X.; Ni, W. X.; Andersson, M. R.; Inganas, O. *Adv. Funct. Mater.* **2009**, *19*, 3293–3299.

(35) Loi, M. A.; Toffanin, S.; Muccini, M.; Forster, M.; Scherf, U.; Scharber, M. *Adv. Funct. Mater.* **2007**, *17*, 2111–2116.